Quantized and unquantized thermal Hall conductance of the Kitaev spin liquid candidate math xmlns="http://www.w3.org/1998/Math/MathML">mi>α/mi>mtext>−/mtext>msub>mrow>mi>RuCl/mi>/mrow>mn>3/mn>/msub>/math>

Y. Kasahara, S. Suetsugu, T. Asaba, S. Kasahara, T. Shibauchi, N. Kurita, H. Tanaka, and Y. Matsuda

Quantized and unquantized thermal Hall conductance of Kitaev spin-liquid candidate α-RuCl$_3$

Y. Kasahara[1], S. Suetsugu[1], T. Asaba[1], S. Kasahara[2], T. Shibauchi[3], N. Kurita[4], H. Tanaka[4], and Y. Matsuda[1]

Department of Physics, Kyoto University, Kyoto 606-8502, Japan
Research Institute for Interdisciplinary Science, Okayama University, Okayama 700-8530, Japan
Department of Advanced Materials Science, University of Tokyo, Chiba 277-8561, Japan and
Department of Physics, Tokyo Institute of Technology, Tokyo 152-8551, Japan

Despite extensive investigations, a topological state that hosts Majorana edge modes in the magnetic field-induced quantum disordered state of Kitaev candidate material α-RuCl$_3$ has been hotly debated. To gain more insight into this issue, we measured the thermal Hall conductivity κ_{xy} of various samples grown by the Bridgman method. The results show that the half-integer quantum thermal Hall effect is intimately related to the magnitude of longitudinal thermal conductivity and the Néel temperature at zero field, both of which are sample-dependent. Samples exhibiting the half-integer quantum thermal Hall effect have larger zero-field thermal conductivity values than a threshold value, implying that a long mean free path of heat carriers is an important prerequisite. In addition, we find that samples with higher Néel temperature exhibit a higher magnetic field at which quantization starts to occur. These results indicate that the quantization phenomenon is significantly affected by the impurity scatterings and the non-Kitaev interactions.

A quantum spin liquid (QSL) is an exotic state of matter in which spins are quantum mechanically entangled over long distances without symmetry-breaking magnetic order [1]. The exactly solvable Kitaev model on the honeycomb lattice has recently received enormous interest in the hope of achieving novel QSL states, where quantum spins are fractionalized into itinerant Majorana fermions and localized Z_2 fluxes (visons) [2]. Recently, α-RuCl$_3$ is drawing much attention as a promising candidate material hosting a Kitaev QSL [3]. The structure of α-RuCl$_3$ consists of edge-sharing RuCl$_6$ octahedra that are stacked along the c axis via van der Waals interaction. This compound is a spin-orbit assisted Mott insulator, in which Ru^{3+} ions have an effective spin-1/2 state forming two-dimensional (2D) honeycomb layers [4]. The spin-orbit coupling and edge-sharing octahedra structure allow bond-dependent Ising interaction between local moments of Ru^{3+} ions [5]. Although α-RuCl$_3$ exhibits an antiferromagnetic (AFM) ordering with zigzag spin structure below the Néel temperature $T_N \sim 7.5\,\mathrm{K}$ due to non-Kitaev interactions, such as Heisenberg exchange and off-diagonal interactions, Kitaev interaction is predominant among the magnetic interactions [6, 7]. The AFM order vanishes by magnetic fields applied parallel to the ab plane, leading to the appearance of a field-induced quantum disordered (FIQD) state above $\sim 8\,\mathrm{T}$.

The fingerprint for Majorana fermions of the fractionalized spin excitations in α-RuCl$_3$ has been reported by several experiments. The specific heat measurements have revealed that the magnitude of the entropy release is quantitatively consistent with the spin-fractionalization [8, 9]. The broad magnetic continuum observed by Raman scattering has been interpreted by the presence of fermionic excitations, in contrast to conventional bosonic magnetic excitations [10]. The inelastic neutron scattering (INS) measurements also reported the magnetic

continuum [8, 11–14], which corresponds to the Kitaev interaction. These results reflect that α-RuCl$_3$ locates in the vicinity of the phase described by the Kitaev model. The Kitaev QSL has topologically protected edge states which are characterized by the Chern number $C_h = \pm 1$ of the Majorana bands. The Chern number is given by the sign of the product $h_x h_y h_z$, where h_x, h_y, and h_z are the x, y, and z components of applied magnetic field $\boldsymbol{H}$ along the *spin* (not crystallographic) axes, respectively. Recently, when magnetic fields are applied tilted from the c axis, half-integer quantized thermal Hall (HIQTH) effect has been reported by several groups [15–18]; the 2D thermal Hall conductance per honeycomb plane $\kappa_{xy}^{\mathrm{2D}}$ shows a quantized plateau behavior as a function of H and has a half value of K_0, where $K_0 = \frac{\pi^2 k_B^2}{3h}T$ is the quantum thermal conductance. The HIQTH conductance provides direct evidence of a non-Abelian phase and topologically protected chiral edge modes of charge-neutral Majorana fermions. Moreover, it has been reported that field-angular variation of the HIQTH conductance has the same sign structure as C_h, $\kappa_{xy}^{\mathrm{2D}} = \frac{1}{2}C_h K_0$ [15]. In particular, for $\boldsymbol{H} \| a$, the planar thermal Hall effect, which is the finite thermal Hall effect for a magnetic field with no out-of-plane components, appears and exhibits a half-quantized plateau. In addition to thermal Hall measurements, recent detailed angle-dependent specific heat measurements have revealed the appearance of an excitation gap Δ_M that increases in proportion to the approximate cube of the magnetic field for $\boldsymbol{H} \| a$, which is consistent with the field dependence of the Majorana gap [21]. In contrast, for $\boldsymbol{H} \| b$, no thermal Hall effect is observed and specific heat measurements report the emergence of quasiparticles that have a gapless linear dispersion [15, 21]. These results suggest that the non-Abelian topological order persists even in the presence of non-Kitaev interactions in α-RuCl$_3$.

However, despite intensive research efforts, the topological properties in α-RuCl$_3$, in particular Majorana excitations, are still under debate, with conflicting results from theoretical and experimental studies. It has been proposed that the magnetic continuum reported by INS can be interpreted by the anharmonic magnons caused by strong magnon-magnon interactions [22, 23]. The HIQTH conductance has been reproduced in some groups [17, 18], but not in others [24–26]. Remarkably, instead of the quantization of κ_{xy}^{2D}, quantum oscillations in the longitudinal thermal conductivity κ_{xx} has been reported both in zigzag AFM and FIQD states [24], suggesting further exotic quantum spin states. In addition, it has been shown that the HIQTH conductance disappears at high fields [15, 16]. This implies that there is a distinct intermediate phase separated from the higher field phase by a topological phase transition within the FIQD state. However, some groups have reported the presence of the intermediate phase [13, 15, 16, 21, 27], while others have claimed the absence of such a phase [28–30].

To shed more light on the above conflicting issues in α-RuCl$_3$, it is crucially important to understand in which samples the HIQTH effect is observed and in which samples it is not. Here, we measured κ_{xy} of various samples. Because it has been shown that different growth methods produce slightly different crystal structures of α-RuCl$_3$ [31], we used one type of crystals, all of which are grown by the same method. We find that the HIQTH effect is observed only in the samples with large longitudinal thermal conductivity in zero field. We also report that the field range at which the quantization occurs is significantly influenced by the Néel temperature that is slightly sample-dependent. We discuss these results in terms of impurity scatterings and non-Kitaev interactions.

Single crystals of α-RuCl$_3$ were grown by the vertical Bridgman method [32]. We measured the crystals taken from the same growth batch as those used in the previous reports [15, 16]. The magnetic susceptibility χ was measured using a SQUID magnetometer and the specific heat C was measured by a long-relaxation time method [33]. We measured the in-plane thermal conductivity κ_{xx} and thermal Hall conductivity κ_{xy} for five crystals using a setup described in Ref. [15]. A heat current $\boldsymbol{q}$ was applied along the a axis. For the measurements of κ_{xy}, magnetic fields $\boldsymbol{H}$ are applied within the ac plane.

In α-RuCl$_3$, the $ABCABC$ stacking arrangement of the 2D layers along the c axis is expected in the trigonal structure, but stacking faults are formed easily and some regions of the sample can crystallize in alternative stacking structures, such as $ABAB$ [34]. It has been shown that $ABAB$-type stacking faults result in additional local magnetic ordering at $T_{N2} \sim 14$ K [32, 34]. Figures 1(a) and (b) show the temperature dependence of magnetic susceptibility for Samples #1-#5 and specific heat for Samples #3 and #5, respectively. As shown in Fig. 1(a), $\chi(T)$ in all crystals shows kink transitions at T_N. While
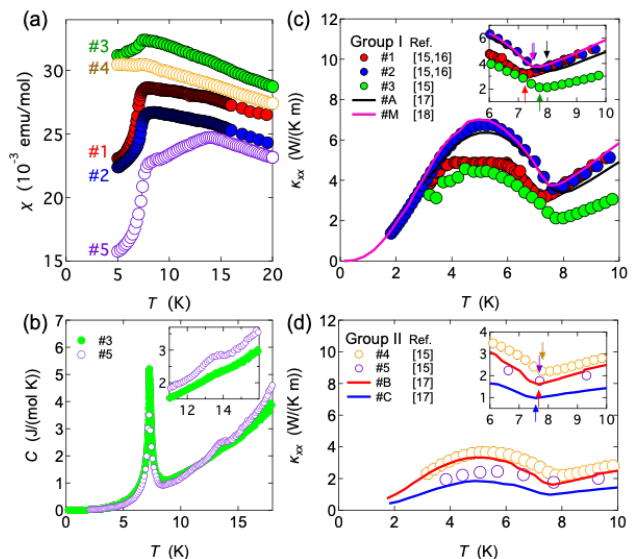
FIG. 1. (a) Temperature dependence of magnetic susceptibility χ under an in-plane magnetic field of 1000 Oe. The data of Samples #3 and #4 are vertically shifted for clarity. All the data are the same data shown in Ref. [15] (χ of Samples #3, #4, and #5 are calculated from the magnetization). (b) Specific heat of Samples #3 and #5 in zero field. The inset shows the data around 14 K. The data of Sample #5 is vertically shifted for clarity. (c), (d) Temperature dependence of κ_{xx}. The data are the same as those reported in Ref. [15]. The solid lines represent the results reported in Refs. [17] and [18]. The insets show κ_{xx} in the vicinity of the Néel temperature, which are shown by arrows.

no distinct anomaly is observed at T_{N2} for Samples #1-#4, Sample #5 exhibits a clear kink anomaly at T_{N2}. The presence of anomaly at T_{N2} in Sample #5 is also confirmed by the specific heat measurements at zero field, while no anomaly is observed in Sample #3, as shown in Fig. 1(b).

Figures 1(c) and 1(d) depict the temperature dependence of κ_{xx} in zero field for Samples #1, #2, and #3 and for Samples #4 and #5, respectively. We note that the magnitude of κ_{xx} varies greatly from sample to sample. Here we divide the samples into two groups according to the magnitude of κ_{xx}, the large ones being Group I shown in Fig. 1(c) and the small ones being Group II shown in Fig. 1(d). In these figures, the results reported in Refs. [17] (Samples #A, #B, and #C) and [18] (Sample #M) are also plotted. For all the samples, κ_{xx} shows a sharp kink at T_N. Such a sharp kink at the transition has been reported in heavy fermion compounds [19, 20]. Below T_N, κ_{xx} increases rapidly with decreasing temperature, peaks at around 5 K, and decreases at lower temperatures. In this temperature range, the phonon contribution is important in the thermal conductivity. Upon entering the AFM state below T_N, the formation of the magnon gap strongly enhances the phonon mean free
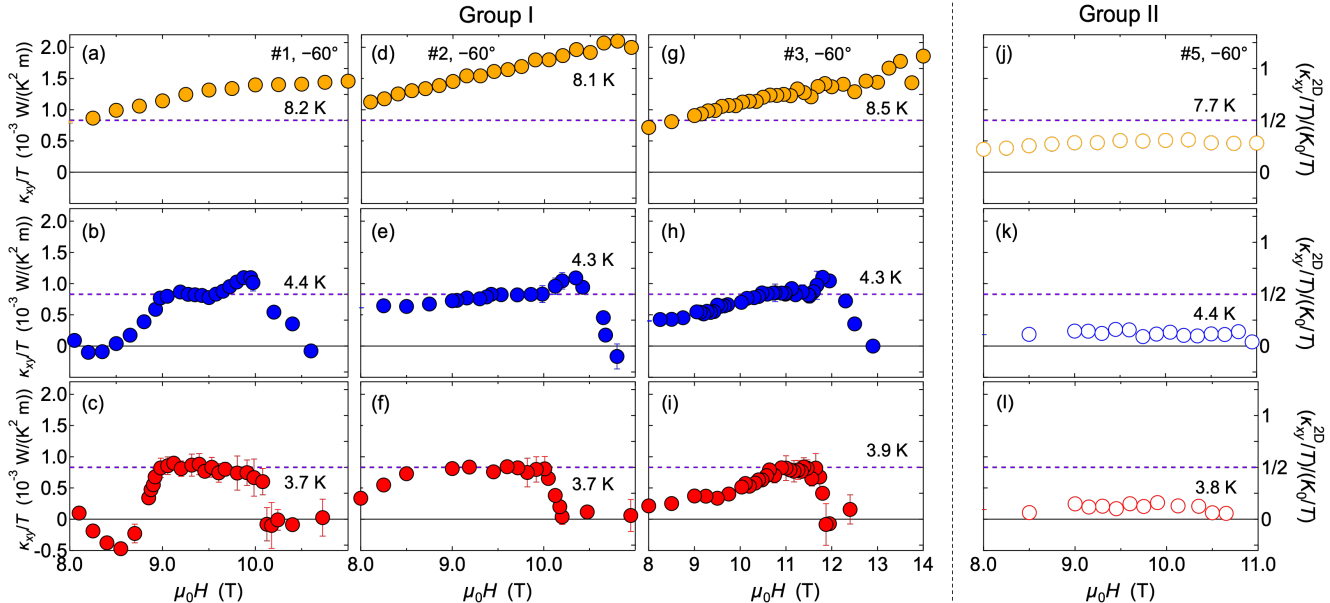
FIG. 2. (a)-(c),(d)-(f), (g)-(i) and (j)-(l) show the field dependence of κ_{xy}/T at $\theta = -60°$ at different temperatures for Samples #1, #2, #3, and #5, respectively. Some of the data (a, b, c, e, h, and k) are the same data reported in Refs. [15] and [16]. The dashed violet lines represent the HIQTH conductance, $\kappa_{xy}^{2D}/T = (K_0/T)/2$.

path through the suppression of magnon-phonon scattering, giving rise to the enhancement of κ_{xx} [17, 35]. Thus the maximum thermal conductivity around 5 K, which is denoted as κ_{xx}^p, measures the mean free path of heat carriers. We point out that the magnitude of κ_{xx}^p is comparable between Samples #4 and #5 regardless of the presence or absence of the stacking faults. This indicates that the absence of the stacking faults does not guarantee the high quality of the samples. Moreover, although it has been proposed that a sample with larger κ_{xx} shows a larger decrease of $\chi(T)$ below T_N [17], such a correlation is not observed in the present experiments (see, for example, $\chi(T)$ and κ_{xx} data of Samples #1 and #2). We also note that the Néel temperatures of each sample can be sensitively detected by the distinct kink of the thermal conductivity, as indicated by arrows in the insets of Figs. 1(c) and (d). To determine T_N accurately, we measured κ_{xx} with a temperature gradient ΔT of 1 % or less of the measured temperature ($\Delta T/T < 0.01$), especially in the vicinity of T_N. We find that the Néel temperature is slightly sample-dependent. Table I lists T_N determined by the thermal conductivity and κ_{xx}^p of Samples #1-5, along with those reported in Refs. [17] and [18].

Figures 2(a)-2(c), 2(d)-2(f), 2(g)-2(i), and 2(j)-2(l) display the magnetic field dependence of κ_{xy}/T for $\theta = -60°$ at several temperatures for Samples #1, #2, #3, and #5, respectively, where θ is the angle between $\boldsymbol{H}$ and the crystallographic c axis. The dashed violet lines rep-

resent the HIQTH conductance, $\kappa_{xy}^{2D}/T = \frac{1}{2}C_h(K_0/T)$ with $C_h = +1$. For Samples #1, #2, and #3, κ_{xy}/T increases with H and is higher than the half quantized value above 8 K. At lower temperatures, κ_{xy}/T exhibits plateau behavior as a function of H in some field ranges

TABLE I. The Néel temperature T_N determined by the thermal conductivity, maximum κ_{xx} below T_N in zero field, κ_{xx}^p (p denotes the peak in κ_{xx}), angle θ between applied magnetic field and the c-axis, and the field range where the plateau of HIQTH conductance is observed in each samples. The results reported in Refs. [17] and [18] are also shown.

Sample	T_N (K)	κ_{xx}^p (W/Km)	θ	plateau field range (T)
Group I (quantized)				
#1	7.2	4.9	$-60°$	9.0-10.1
#1			$-45°$	9.4-10.4
#2	7.6	6.7	$-60°$	9.4-10.0
#3	7.7	4.5	$-60°$	10.5-11.6
#3			$+60°$	10.5-13.2
#3			$-90°$	9.9-11.3
#A [17]	7.9	6.4	$+45°$	12.1-12.7
#M [18]	7.5	7.0	$-70°$	
Group II (unquantized)				
#4	7.8	3.7	$-60°$	
#5	7.7	2.5	$-60°$	
#B [17]	7.7	3.3	$+45°$	
#C [17]	7.6	1.8	$+45°$	
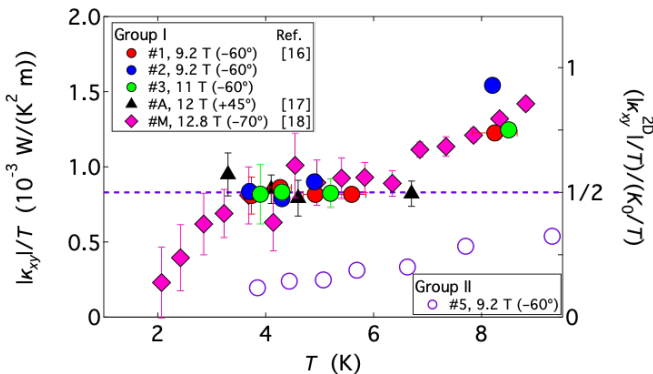
FIG. 3. Temperature dependence of $|\kappa_{xy}|/T$ for six different α-RuCl$_3$ crystals. The dashed violet lines represent the HIQTH conductance, $\kappa_{xy}^{2D}/T = (K_0/T)/2$.
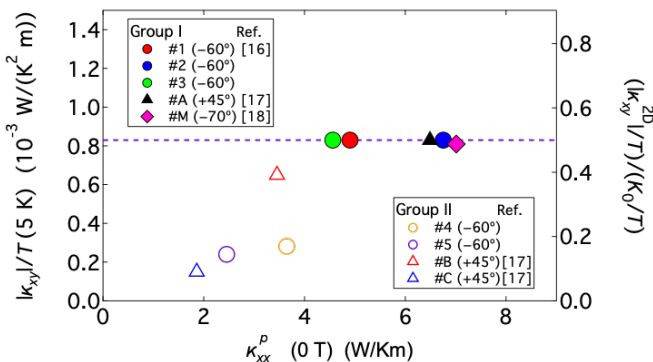
FIG. 4. $|\kappa_{xy}|/T$ in the plateau region plotted as a function of maximum κ_{xx} below T_N in zero field, κ_{xx}^p (p denotes the peak in κ_{xx}).

and its value is very close to the HIQTH conductance. The plateau field range of Sample #2 is similar to Sample #1 but is slightly lower than that of Sample #3. A possible origin of this difference will be discussed later. In contrast to Samples #1, #2, and #3, κ_{xy}/T of Sample #5 is smaller than the half-quantized value in the whole temperature range. Thus, the samples belonging to Group I exhibit HIQTH conductance, while those in Group II do not show the quantization.

Figure 3 shows the temperature dependence of $|\kappa_{xy}|/T$ at the fields where the HIQTH effect is observed. Results reported in Refs. [17] and [18] are also shown for comparison (#A and #M). For all the samples that belong to Group I, $|\kappa_{xy}|/T$ shows similar temperature dependence. As the temperature decreases from high temperatures, $|\kappa_{xy}|/T$ decreases. Half-integer quantization is observed around 6.5 K and continues down to around 3.5 K. At even lower temperatures, it has been reported that $|\kappa_{xy}|/T$ is reduced to be smaller than the half-integer quantization value, as shown by the data for Sample #M.

In contrast, for samples that belong to Group II, T dependence of $|\kappa_{xy}|/T$ is essentially different from that of Group I; $|\kappa_{xy}|/T$ decreases monotonically with decreasing T, and its value is smaller than the half-quantized value in the whole temperature range. We note that similar T-dependence has been reported in the samples grown by the chemical vapor transport method with similar κ_{xx}^p values to those of Group II and no quantization has been observed [24, 25]. This suggests that the sample quality plays an important role in the HIQTH effect. However, since the preparation method of the samples is different, a simple comparison should be made with caution. The enhancement of $|\kappa_{xy}|/T$ from the half-quantized value at high temperatures has been attributed to excitations of visons and different types of Majorana fermions in addition to Majorana edge currents [36]. The reduction from the half-quantized value at low temperatures has been discussed in terms of the decoupling phenomena between phonons and Majorana edge currents [37, 38].

In Fig. 4, we plot $|\kappa_{xy}|/T$ at 5 K, where the HIQTH effect is observed, as a function of κ_{xx}^p. Although it has been qualitatively suggested that samples with higher κ_{xx} tend to exhibit the HIQTH effect [15, 17], the present results obtained using the samples from the same batch demonstrate that there is a threshold value $\kappa_{xx}^p \sim 4$ W/Km above which the quantization occurs. The presence of threshold value of κ_{xx}^p is clearly seen by comparing Samples #3 and #4; Sample #3 with $\kappa_{xx}^p = 4.5$ W/Km exhibits the HIQTH effect, while Sample #4 with $\kappa_{xx}^p = 3.7$ W/Km does not. For samples with smaller values (Group-II), no quantization is observed, and $|\kappa_{xy}|/T$ at 5 K decreases with decreasing κ_{xx}^p. This suggests that low scattering by impurities and defects is intrinsically important to yield the quantization of the thermal Hall effect. Very recently, the disorder effect on the Kitaev spin liquid has been argued theoretically [39–41]. It has been shown that the half quantization of κ_{xy} is fragile against the site dilution [39], which appears to be consistent with the present results.

We here comment on the phonon thermal Hall effect. The observation of the planar thermal Hall effect [15, 24] and the sign change of κ_{xy} with magnetic field rotation [15] cannot be explained by phonon scenario, but consistent with the Kitaev model. Phonon scenario has been claimed based on the results that the temperature dependence of κ_{xy} is similar to that of κ_{xx} for $\boldsymbol{H} \parallel c$ below and above T_N; both κ_{xx} and κ_{xy} exhibit a clear upturn at T_N [26]. In sharp contrast, however, as reported in Refs. [42, 43], while κ_{xx} exhibits a clear upturn, κ_{xy} only changes its sign without showing upturn, reporting the absence of the trend claimed in Ref. [26].

We finally discuss the magnetic field range where the HIQTH plateau is observed. In Fig. 5(a), the field range of the plateau at three different angles for Sample #3 is shown by the green bars. The lower boundary of the plateau does not depend much on the angle, but
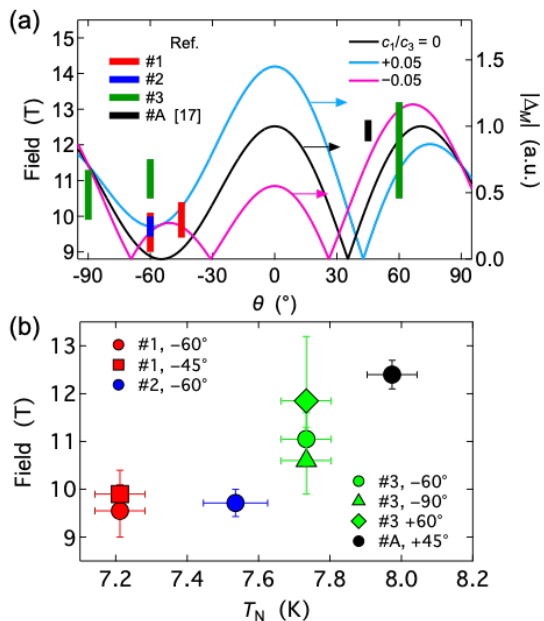
FIG. 5. (a) The red, blue, green and black bars represent the field range (left axis) where the plateau of HIQTH conductance is observed for Samples #1, #2, #3, and #A (Ref. [17]), respectively. Black solid line represent the Majorana gap $|\Delta_M|$ (right axis) in the absence of non-Kitaev interactions. Light blue and pink solid lines represent $|\Delta_M|$ in the presence of non-Kitaev interaction for $c_1/c_3 = +0.05$ and -0.05, respectively. (b) The quantization field vs. T_N for Samples #1, #2, #3, and #A (Ref. [17]). The symbols represent the mid-points of the plateau field, and error bars represent the onset and offset fields for the HIQTH plateau.

the upper boundary is distinctly higher at $+60°$ than at $-90°$ or $-60°$. In the presence of non-Kitaev interactions, such as Heisenberg and off-diagonal exchanges, the Chern number is written as, $C_h = \text{sgn}\{c_1(h_x + h_y + h_z) + c_3(h_x h_y h_z) + \cdots\}$, where c_1 and c_3 terms represent the contributions of the non-Kitaev and Kitaev terms, respectively [15]. In this case, the Majorana gap is written as $\Delta_M/c_3 = (c_1/c_3)(h_x+h_y+h_z)+(h_x h_y h_z)$. In Fig. 5(a), angular variation of $|\Delta_M|$ for pure Kitaev model with $c_1 = 0$ and in the presence of non-Kitaev interactions with $c_1/c_3 = \pm 0.05$ are shown by solid lines. For all c_1 values, $|\Delta_M|$ takes a maximum at $\theta \sim +60°$. Although a more accurate theory incorporating the non-Kitaev terms is needed to calculate the detailed angular dependence, the higher upper boundary at $\theta = +60°$ may be related to the larger $|\Delta_M|$.

In Fig. 5(a), we also plot the magnetic field range of the plateau for Samples #1 (red) and #2 (blue), along with the data reported in Ref. [17]. The field range of the quantization is sample-dependent. We note that as shown in Fig. 1(c), the Néel temperature is also sample dependent. To examine the correlation between the quantization field and Néel temperature, the quantiza-

tion field is plotted against T_N in Fig. 5(b). Notably, the sample with higher Néel temperature tends to have a higher onset field of the quantization. As the Néel temperature is determined by the Kitaev and non-Kitaev interactions, the results suggest that the difference of the plateau fields appears to be associated with the slightly sample-dependent Kitaev and non-Kitaev interactions. While further studies are warranted, the present results provide an important clue to the origin of the sample-dependent quantization field.

In summary, we have measured κ_{xy} of various samples grown by the Bridgman method. The results show that there is a relationship between the HIQTH effect and the thermal conductivity in zero fields. Samples exhibiting the HIQTH effect have larger zero-field longitudinal thermal conductivity below and above the Néel temperature than those not exhibiting quantization. In the unquantized samples, $|\kappa_{xy}|/T$ is always smaller than the quantized value and decreases monotonically with decreasing temperature in the FIQD state. In addition, we find that the onset field of the quantization is nearly angular independent in the same sample but distinctly depends on slightly sample-dependent Néel temperature. The samples with higher Néel temperature exhibit higher quantization fields. These results indicate that the quantization phenomenon is significantly influenced by the impurity/defect scatterings and the non-Kitaev interactions.

[1] L. Balents, Nature **464**, 199-208 (2010).
[2] A. Kitaev, Ann. Phys. **321**, 2-111 (2006).
[3] H. Takagi, T. Takayama, G. Jackeli, G. Khaliullin, and S. E. Nagler, Nat. Rev. Phys. **1**, 264-280 (2019).
[4] K. W. Plumb, J. P. Clancy, L. J. Sandilands, V. V. Shankar, Y. F. Hu, K. S. Burch, H. Y. Kee, and Y. J. Kim, Phys. Rev. B **90**, 041112(R) (2014).
[5] G. Jackeli and G. Khaliullin, Phys. Rev. Lett. **102**, 017205 (2009).
[6] Y. Motome and J. Nasu, J. Phys. Soc. Jpn. **89**, 012002 (2020).
[7] S. M. Winter, A. A. Tsirlin, M. Daghofer, J. van den Brink, Y. Singh, P. Gegenwart, and R. Valentí, J. Phys.: Condens. Matter **29**, 493002 (2017).
[8] S.-H. Do, S.-Y. Park, J. Yoshitake, J. Nasu, Y. Motome, Y. S. Kwon, D. T. Adroja, D. J. Voneshen, K. Kim, T.-H. Jang, J.-H. Park, K.-Y. Choi, and S. Ji, Nat. Phys. **13**, 1079-1084 (2017).
[9] S. Widmann, V. Tsurkan, D. A. Prishchenko, V. G.

Mazurenko, A. A. Tsirlin, and A. Loidl, Phys. Rev. B **99**, 094415 (2019).

[10] L. J. Sandilands, Y. Tian, K. W. Plumb, Y. J. Kim, and K. S. Burch, Phys. Rev. Lett. **114**, 147201 (2015).

[11] A. Banerjee, C. A. Bridges, J.-Q. Yan, A. A. Aczel, L. Li, M. B. Stone, G. E. Granroth, M. D. Lumsden, Y. Yiu, J. Knolle, S. Bhattacharjee, D. L. Kovrizhin, R. Moessner, D. A. Tennant, D. G. Mandrus, and S. E. Nagler, Nat. Mater. **15**, 733-740 (2016).

[12] A. Banerjee, P. Lampen-Kelley, J. Knolle, C. Balz, A. A. Aczel, B. Winn, Y. Liu, D. Pajerowski, J. Yan, C. A. Bridges, A. T. Savici, B. C. Chakoumakos, M. D. Lumsden, D. A. Tennant, R. Moessner, D. G. Mandrus, and S. E. Nagler, npj Quant. Meter. **3**, 8 (2018).

[13] C. Balz, P. Lampen-Kelley, A. Banerjee, J. Yan, Z. Lu, X. Hu, S. M. Yadav, Y. Takano, Y. Liu, D. A. Tennant, M. D. Lumsden, D. Mandrus, and S. E. Nagler, Phys. Rev. B **100**, 060405(R) (2019).

[14] K. Ran, J. Wang, S. Bao, Z. Cai, Y. Shangguan, Z. Ma, W. Wang, Z.-Y. Dong, P. Çermák, A. Schneidewind, S. Meng, Z. Lu, S.-L. Yu, J.-X. Li, and J. Wen, Chinese Phys. Lett. **39**, 027501 (2022).

[15] T. Yokoi, S. Ma, Y. Kasahara, S. Kasahara, T. Shibauchi, N. Kurita, H. Tanaka, J. Nasu, Y. Motome, C. Hickey, S. Trebst, and Y. Matsuda, Science **373**, 568-572 (2021).

[16] Y. Kasahara, T. Ohnishi, Y. Mizukami, O. Tanaka, S. Ma, K. Sugii, N. Kurita, H. Tanaka, J. Nasu, Y. Motome, T. Shibauchi, and Y. Matsuda, Nature **559**, 227-231 (2018).

[17] M. Yamashita, J. Gouchi, Y. Uwatoko, N. Kurita, and H. Tanaka, Phys. Rev. B **102**, 220404(R) (2020).

[18] J. A. N. Bruin, R. R. Claus, Y. Matsumoto, N. Kurita, H. Tanaka, and H. Takagi, Nat. Phys. (2022).

[19] K. Izawa, H. Yamaguchi, Y. Matsuda, H. Shishido, R. Settai, and Y. Onuki, Phys. Rev. Lett. **87**, 057002 (2001).

[20] K. Behnia, R. Bel, Y. Kasahara, Y. Nakajima, H. Jin, H. Aubin, K. Izawa, Y. Matsuda, J. Flouquet, Y. Haga, Y. Onuki, and P. Lejay, Phys. Rev. Lett. **94**, 156405 (2005).

[21] O. Tanaka, Y. Mizukami, R. Harasawa, K. Hashimoto, K. Hwang, N. Kurita, H. Tanaka, S. Fujimoto, Y. Matsuda, E.-G. Moon, and T. Shibauchi, Nat. Phys. (2022).

[22] S. M. Winter, K. Riedl, P. A. Maksimov, A. L. Chernyshev, A. Honecker, and R. Valentí, Nat. Commun. **8**, 1152 (2017).

[23] P. A. Maksimov and A. L. Chernyshev, Phys. Rev. Research **2**, 033011 (2020).

[24] P. Czajka, T. Gao, M. Hirshberger, P. Lampen-Kelley, A. Banerjee, J. Yan, D. G. Mandrus, S. E. Nagler, and N. P. Ong, Nat. Phys. **17**, 915-919 (2021).

[25] P. Czajka, T. Gao, M. Hirshberger, P. Lampen-Kelley, A. Banerjee, N. Quirk, D. G. Mandrus, S. E. Nagler, and N. P. Ong, arXiv:2201.07873 (2022).

[26] É. Lefrançois, G. Grissonnanche, J. Baglo, P. Lampen-Kelley, J. Yan, C. Balz, D. Mandrus, S. E. Nagler, S. Kim, Y.-J. Kim, N. Doiron-Leyraud, and L. Taillefer, arXiv:2111.05493 (2021).

[27] S. Suetsugu, Y. Ukai, M. Shimomura, M. Kamimura, T. Asaba, Y. Kasahara, N. Kurita, H. Tanaka, T. Shibauchi, J. Nasu, Y. Motome, and Y. Matsuda, arXiv:2203.00275 (2022).

[28] S. Bachus, D. A. S. Kaib, A. Jesche, V. Tsurkan, A. Loidl, S. M. Winter, A. A. Tsirlin, R. Valentí, and P. Gegenwart, Phys. Rev. B **103**, 054440 (2021).

[29] K. A. Modic, R. D. McDonald, J. P. C. Ruff, M. D. Bachmann, Y. Lai, J. C. Palmstrom, D. Graf, M. K. Chan, F. F. Balakirev, J. B. Betts, G. S. Boebinger, M. Schmidt, M. J. Lawler, D. A. Sokolov, P. J. W. Moll, B. J. Ramshow, and A. Shekhter, Nat. Phys. **17**, 240-244 (2021).

[30] A. N. Ponomaryov, L. Zviagina, J. Wosnitza, P. Lampen-Kelley, A. Banerjee, J. Q. Yan, C. A. Bridges, D. G. Mandrus, S. E. Nagler, and S. A. Zvyagin, Phys. Rev. Lett. **125**, 037202 (2020).

[31] J. A. N. Bruin, R. R. Claus, Y. Matsumoto, J. Nuss, S. Laha, B. V. Lotsch, N. Kurita, H. Tanaka, and H. Takagi, arXiv:2205.15839 (2022).

[32] Y. Kubota, H. Tanaka, T. Ono, Y. Narumi, and K. Kindo Phys. Rev. B **91**, 094422 (2015).

[33] O. J. Taylor, A. Carrington, and J. A. Schlueter, Phys. Rev. Lett. **99**, 057001 (2007).

[34] H. B. Cao, A. Banerjee, J. Q. Yan, C. A. Bridges, M. D. Lumsden, D. G. Mandrus, D. A. Tennant, B. C. Chakoumakos, and S. E. Nagler, Phys. Rev. B **93**, 134423 (2016).

[35] R. Hentrich, A. U. B. Wolter, X. Zotos, W. Brenig, D. Nowak, A. Isaeva, T. Doert, A. Banerjee, P. Lampen-Kelley, D. G. Mandrus, S. E. Nagler, J. Sears, Y. J. Kim, B. Buchner, and C. Hess, Phys. Rev. Lett. **120**, 117204 (2018).

[36] A. Go, J. Jung, and E.-G. Moon, Phys. Rev. Lett. **122**, 147203 (2019).

[37] Y. Vinkler-Aviv and A. Rosch, Phys. Rev. X **8**, 031032 (2018).

[38] M. Ye, G. B. Halász, L. Savary, and L. Balents, Phys. Rev. Lett. **121**, 147201 (2018).

[39] J. Nasu and Y. Motome, Phys. Rev. B **102**, 054437 (2020).

[40] M. G. Yamada, npj Quantum Mater. **5**, 82 (2020).

[41] J. Nasu and Y. Motome, Phys. Rev. B **104**, 035116 (2021).

[42] Y. Kasahara, K. Sugii, T. Ohnishi, M. Shimozawa, M. Yamashita, N. Kurita, H. Tanaka, J. Nasu, Y. Motome, T. Shibauchi, and Y. Matsuda Phys. Rev. Lett. **120**, 217205 (2018).

[43] R. Hentrich, M. Roslova, A. Isaeva, T. Doert, W. Brenig, B. Buchner, and C. Hess, Phys. Rev. B **99**, 085136 (2019).